Available online at www.sciencedirect.com
ScienceDirect
Trans. Nonferrous Met. Soc. China 32(2022) 895−907
Transactions of Nonferrous Metals Society of China
www.tnmsc.cn

Prediction of low-cycle crack initiation life of powder superalloy FGH96 with inclusions based on damage mechanics

Yuan-ming XU[1], Shu-ming ZHANG[1], Tian-peng HE[1], Xin-ling LIU[2], Xia-yuan CHANG[1]

1. School of Aeronautic Science and Engineering, Beihang University, Beijing 100191, China;
2. AECC Beijing Institute of Aeronautical Materials, Beijing 100095, China

Received 9 March 2021; accepted 9 October 2021

Abstract: The effects of inclusions in powder superalloy FGH96 on low-cycle fatigue life were studied, and a low-cycle crack initiation life prediction model based on the theory of damage mechanics was proposed. The damage characterization parameter was proposed after the construction of damage evolution equations. Fatigue tests of the powder superalloy specimens with and without inclusion were conducted at 530 and 600 °C, and the model verification was carried out for specimens with elliptical, semi-elliptical, polygon and strip-shaped surface/subsurface inclusion. The stress analysis was performed by finite element simulation and the predicted life was calculated. The results showed a satisfying agreement between predicted and experimental life.

Key words: powder superalloy FGH96; low-cycle fatigue; inclusion; crack initiation life prediction; damage mechanics

1 Introduction

Powder superalloys are widely applied in the manufacture of high-temperature bearing rotating parts such as turbine disks of advanced aero-engines, due to their excellent mechanical properties [1−3]. In the process of preparation and collection of powder, however, a large number of non-metallic inclusions and ceramic particles are inevitably mixed. Under the cyclic loading, these pre-existing defects tend to become fatigue crack initiation points, which reduce fatigue life and increase the dispersion of life [4−6]. Therefore, in order to continuously improve the reliability and safety of engine turbine disk, it is indispensable to develop efficient life prediction of turbine disk including inclusions with high accuracy.

The method which is most commonly used for low-cycle fatigue design of the turbine disks in USA and UK is the safe life design method. MANSON [7] and COFFIN [8] proposed the empirical relationship between plastic strain amplitude and fatigue life, namely the Manson−Coffin formula, and thus local stress−strain method was formed. However, the fatigue life prediction model based on the Manson−Coffin equation could not be applied in the fatigue life prediction of superalloy containing powder inclusions due to obvious characteristics of high strength and low plasticity, which led to large calculation errors in the plastic part of the Manson−Coffin equation. HU et al [9] proposed a modified Manson−Coffin equation for FGH96 including inclusion parameters and obtained the crack nucleation region diameter through the post-test fractography examination. The results showed that the powder metallurgy FGH96 superalloy was sensitive to surface scratches, surface inclusion and other surface defects. CHEN [10] studied the effect of inclusions on stress intensity factors in FGH95 superalloy by finite

Corresponding author: Tian-peng HE, Tel: +86-13811947667, E-mail: hetianpg@126.com
DOI: 10.1016/S1003-6326(22)65845-X

element method, and the results showed that the stress intensity factors of inclusion cracking and debonding at inclusion/matrix interface were less than those of considering inclusions as initial cracks. MIAO et al [11] investigated FGH96 fatigue behavior at 600 °C and reported the negative effect of inclusions at the specimen surface.

Moreover, due to the inhomogeneity of inclusion distribution and the fluctuation based on experimental observation, the fatigue life of powder superalloy showed obvious scattering characteristic [12−14]. Considering this variability, the uncertainty of the life model such as the Bayesian method was usually used in the fatigue life prediction to replace the traditional safety factor [15−17]. JIANG et al [18,19] stated that fatigue life of turbine disk alloy N18 appeared to be dominated by crack initiation process. SONG and GAO [20] studied the failure mechanism of low-cycle fatigue of powder metallurgy turbine disk, proposing that the stress distribution around inclusions had an important influence on crack initiation and early propagation. The negative effects of inclusions on the specimen were reported. ZHANG et al [21] constructed a new low-cycle fatigue life prediction model considering the effect of grain size, achieving a higher prediction accuracy than Manson−Coffin relationship and Ostergren energy approach. In addition, some researchers [22,23] studied the propagation rate model of short crack in powder superalloy, and obtained the conclusion that the propagation law of short crack was similar to that of the long crack. CHAN [24] analyzed the conditions for the concurrent occurrence of fatigue crack nucleation at inclusions and slipbands, and calculated fatigue crack nucleation cycles at inclusions in nickel-based superalloy based on fatigue theory. Nevertheless, fatigue theory is based on the ideal material assumption, so the existence of defects does not conform to the precondition of fatigue theory. SHI et al [25] conducted fatigue tests in several conditions, the results of which showed that the existence of surface defects greatly shortened fatigue life. Based on the fracture mechanics, a life prediction method was proposed, which was checked for application in other loading conditions. However, the accuracy of fracture−mechanics based life prediction method is insufficient and cannot reflect the influence of different defect characteristics on crack initiation life.

Therefore, based on the theory of damage mechanics, a method for predicting the fatigue crack initiation life of powder superalloys was proposed in this work. This method considers local stress and strain, and thus it can predict not only the life of powder superalloy materials without micro-defects, but also the life of powder superalloy materials with micro-defects (inclusions, etc). The damage characterization parameter was defined and the damage evolution equation was derived. A specific method for the fatigue life prediction of powder superalloy based on the damage evolution equation was then proposed. Finally, the fatigue lives of powder superalloy specimens with different kinds of inclusions were predicted. The applicability of the model was verified by comparing the predicted results with the experimental results.

2 Method for predicting crack initiation life of powder superalloy

2.1 Damage characterization parameter definition and damage evolution equation

Based on the thermodynamic theory of damage mechanics, the damage characterization parameter Y is defined, which can characterize material damage failure. Its physical meaning is the free energy dissipation rate caused by damage [26]. Thus, it can be seen that the damage reduces the part of the internal energy that can work outside, and dissipates it in the form of heat. Therefore, damage is a process of energy devaluation, and it also must be an irreversible one-way process.

Firstly, the damage field of the material crack initiation life around the inclusions is defined as follows:

$$D(x_i, N) = \frac{E - E_D(x_i, N)}{E} \tag{1}$$

where E is the elastic modulus of the powder superalloy. E_D is the macroscopic equivalent modulus after damage caused by local mesoscopic defects; the damage field D ranges from 0 to 1. When it is 0, this indicates that the material does not begin to damage. When it is 1, it indicates macroscopic crack initiation. x_i indicates spatial position coordinates, and N is the cycle number. The damage field is a scalar field, which is a

function of cycle times and spatial position. The distribution of different locations of the material changes with time.

Then, the constitutive equation of material with damage can be expressed as

$$\varepsilon_{ij}=\frac{1}{1-D}C_{ijkl}\sigma_{kl} \tag{2}$$

where ε_{ij} is the strain component, σ_{kl} is the stress component, and C_{ijkl} is the fourth-order flexibility tensor component.

According to theory of damage mechanics, the damage process of the powder superalloy material is regarded as an irreversible thermodynamic process. In this process, the unit mass free energy g can be expressed as

$$g=\frac{\sigma_{ij}\varepsilon_{ij}}{2\rho}=\frac{C_{ijkl}\sigma_{kl}\sigma_{ij}}{2\rho(1-D)} \tag{3}$$

where ρ is the material density.

The damage characterization parameter Y can be expressed as

$$Y=-\rho\frac{\partial g}{\partial D}=\frac{C_{ijkl}\sigma_{kl}\sigma_{ij}}{2(1-D)^2} \tag{4}$$

The time-type damage evolution equation can be written as

$$\frac{\mathrm{d}D}{\mathrm{d}t}=bY^{\frac{m}{2}-1}\frac{\mathrm{d}Y}{\mathrm{d}t} \tag{5}$$

where b is the coefficient of the exponential function and m is the exponential related parameter and their specific values need to be fitted according to fatigue experimental data. The equation demonstrates that the increment of damage degree per unit time is exponentially related to the damage characterization parameters.

It is evident from Eq. (4) that characterization parameter Y is non-negative. Therefore, there are two cases during cyclic loading, as shown in Fig. 1. For the fatigue problem under uniaxial tensile and compressive load, the first case corresponds to tension−tension loading, while the second case refers to tension−compression loading.

For the first case, we define

$$r_+=\sqrt{\frac{Y_{\min}}{Y_{\max}}}>0 \tag{6}$$

And for the second case, we define

$$r_-=-\sqrt{\frac{Y_{\min}}{Y_{\max}}}<0 \tag{7}$$

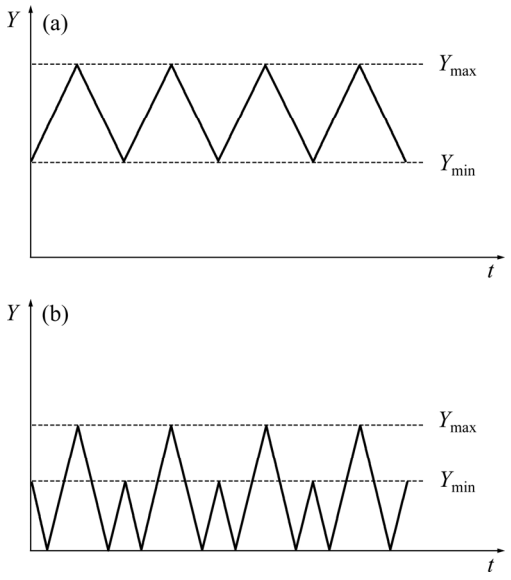

Fig. 1 Two cases of characterization parameter Y during cyclic loading

Since there is a quadratic relationship between the damage characterization parameter Y and the stress−strain, then for the above two cases, the damage evolution equations of cyclic type can be obtained by integral of Eq. (5) as

$$\frac{\mathrm{d}D}{\mathrm{d}N}=\int_0^{t_{\max}}\frac{\mathrm{d}D}{\mathrm{d}t}\mathrm{d}t=a(Y_{\max}^{m/2}-Y_{\min}^{m/2})=a(1-r_+^m)Y_{\max}^{m/2} \tag{8}$$

$$\frac{\mathrm{d}D}{\mathrm{d}N}=\int_0^{t_{\max}}\frac{\mathrm{d}D}{\mathrm{d}t}\mathrm{d}t+\int_0^{t_{\min}}\frac{\mathrm{d}D}{\mathrm{d}t}\mathrm{d}t=a(Y_{\max}^{m/2}+Y_{\min}^{m/2})=a(1+|r_-|^m)Y_{\max}^{m/2} \tag{9}$$

where $a=2b/m$.

The meaning of this equation is that the increase in damage caused by the cycle of unit fatigue load has an exponential function relationship with the damage characterization parameter, where a is the coefficient of the exponential relationship. Only two of the three damage parameters a, b and m are independent, so only two of them are needed when fitting the parameters.

The specific formulas of Y for this research expanding from Eqs. (4) can be described as

$$Y=\frac{W}{1-D}=\frac{\mu E}{2(1+\mu)(1-2\mu)}\left(\varepsilon_x+\varepsilon_y+\varepsilon_z\right)^2+\frac{E}{2(1+\mu)}\left[\varepsilon_x^2+\varepsilon_y^2+\varepsilon_z^2+\frac{1}{2}\left(\gamma_{xy}^2+\gamma_{yz}^2+\gamma_{zx}^2\right)\right] \tag{10}$$

where W is the strain energy density; μ is the Poisson's ratio; $\varepsilon_{i,j}$ and γ_{ij} are strain components.

Substituting Eqs. (10) into Eqs. (8) and (9), we have

$$\frac{\mathrm{d}D}{\mathrm{d}N}=\frac{aRW_{\max}^{m/2}}{(1-D)^{m/2}}=a(Y_{\max}^{m/2}\mp Y_{\min}^{m/2})=aRY_{\max}^{m/2} \tag{11}$$

The sign is negative in the tension−tension loading and the cycle characteristic parameter R is defined as

$$R=\begin{cases}1-r_{+}^{m} & \text{(case 1)}\\ 1+\left|r_{-}\right|^{m} & \text{(case 2)}\end{cases} \tag{12}$$

The damage evolution equation above was embedded in the finite element software for secondary development. In the finite element software, the geometric size and material parameters of the actual specimen were installed to establish the corresponding computation model, and load boundary conditions were applied. When the solution was used to calculate the damage characterization parameters, the cloud chart representing the parameter field Y could be obtained, and the crack initiation position information could be obtained according to the cloud chart. By substituting the damage characteristic parameters of the critical point into the damage evolution equation, the fatigue life could be calculated.

2.2 Fitting of damage parameters

To predict the fatigue life of powder superalloy using the damage evolution equation, it is necessary to fit the undetermined parameters a and m in the equation. The parameter fitting method needs the test data under the pulsating constant amplitude load spectrum, so the sign between the maximum characterization parameter $Y_{\max}$ and the minimum characterization parameter $Y_{\min}$ is uniformly subtracted in this section.

Substitute Eq. (10) into Eq. (11) and simplify it in the form of maximum cyclic strain:

$$\frac{\mathrm{d}D}{\mathrm{d}N}=a(Y_{\max}^{m/2}-Y_{\min}^{m/2})=aRY_{\max}^{m/2}=$$
$$aR\left\{\frac{\mu E}{2(1+\mu)(1-2\mu)}(\varepsilon_x+\varepsilon_y+\varepsilon_z)^2+\right.$$
$$\left.\frac{E}{2(1+\mu)}\left[\varepsilon_x^2+\varepsilon_y^2+\varepsilon_z^2+\frac{1}{2}(\gamma_{xy}^2+\gamma_{yz}^2+\gamma_{zx}^2)\right]\right\}^{m/2} \tag{13}$$

The damage parameters a and m in the formula are determined by fitting the fatigue experimental data of standard smooth specimens. The strain component at each load component takes the maximum load, and the influence of the minimum load is reflected in the cyclic characteristic factor R. For the uniaxial load fatigue test of standard smooth specimens without inclusions, there is only one strain component, and Eq. (13) is simplified to

$$\frac{\mathrm{d}D}{\mathrm{d}N}=a\left(\frac{E}{2}\right)^{m/2}(\varepsilon_{\max}^{m}-\varepsilon_{\min}^{m})=aR\left(\frac{E}{2}\right)^{m/2}\varepsilon_{\max}^{m} \tag{14}$$

This formula is integrated over the load history and takes the logarithm:

$$\lg N=\lg C-m\lg\varepsilon_{\max} \tag{15}$$

where $C=1/[aR(E/2)^{m/2}]$.

According to the fatigue life data at different strain levels obtained from the fatigue test of standard smooth specimens, parameters m and C can be determined by linear regression. The error function of the least squares method is defined as

$$\Phi=\sum_{i=1}^{n}\left[\lg N_i-\lg N(\varepsilon_{\max,i})\right]^2 \tag{16}$$

For the powder superalloy FGH96 material, the damage parameters m and C were fitted with fatigue test data with three strain ranges at 530 °C. The experimental conditions were uniaxial tension−tension loading and controlled strain loading. The three strain ranges were 0.95%, 0.75% and 0.846%, and the loading strain ratio was r=0.05.

The fatigue test data of the standard smooth test specimens at 530 °C are listed in Table 1. All the test specimens were tested as standard smooth fatigue bars without meso defects. The data were substituted into Eq. (16) to take the minimum value, and the fitting curve is shown in Fig. 2. It can be found from Fig. 2 that the scatter of the experimental results is large, which can be attributed to the inhomogeneity of inclusion distribution and the fluctuation based on experimental observation [12−14]. Subsequently, by fitting the fatigue test data of the standard smooth piece without inclusions, the damage parameters of the FGH96 material at 530 °C are determined as m=5.594 and lg C=−7.48.

Table 1 Fatigue test data of powder superalloy FGH96 without inclusions at 530 °C

No.	Strain range/%	Strain ratio	Maximum strain	Cycle number	Diameter/mm
1	0.95	0.05	0.01	6235	6
2	0.95	0.05	0.01	5842	6
3	0.95	0.05	0.01	3700	6
4	0.95	0.05	0.01	4988	6
5	0.95	0.05	0.01	6890	6
6	0.95	0.05	0.01	2880	6
7	0.95	0.05	0.01	4560	6
8	0.95	0.05	0.01	4756	6
9	0.76	0.05	0.008	8765	6
10	0.76	0.05	0.008	25615	6
11	0.76	0.05	0.008	10985	6
12	0.76	0.05	0.008	11970	6
13	0.76	0.05	0.008	14042	6
14	0.76	0.05	0.008	21724	6
15	0.76	0.05	0.008	14426	6
16	0.846	0.05	0.0089	8301	6
17	0.846	0.05	0.0089	14521	6
18	0.846	0.05	0.0089	11031	6
19	0.846	0.05	0.0089	10454	6
20	0.846	0.05	0.0089	11518	6
21	0.846	0.05	0.0089	11376	6
22	0.846	0.05	0.0089	12900	6
23	0.846	0.05	0.0089	6567	6

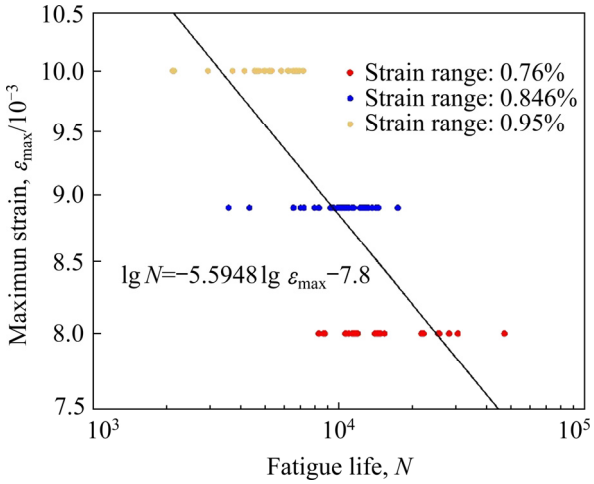

Fig. 2 Fitting curve of FGH96 damage parameters at 530 °C

According to Eq. (15), there is

$$a=1/[CR(E/2)^{m/2}] \tag{17}$$

Since m=5.594, according to the definition of the cycle characteristic R, there is

$$R=1-r^m=1-0.05^{5.594}\approx 1 \tag{18}$$

Then, $a=1/[CR(E/2)^{m/2}]=3.8702\times10^{-7}$. So far, the damage parameters of FGH96 material at 530 °C have been obtained. These parameters can be used to predict the crack initiation life of the material at 530 °C.

Similarly, the damage parameters of FGH96 at 600 °C are determined as m=6.282, lg C=−8.562, and $a=1/[CR(E/2)^{m/2}]=9.1442\times10^{-8}$ according to Table 2 and Fig. 3.

Table 2 Fatigue test data of powder superalloy FGH96 without inclusions at 600 °C

No.	Strain range/%	Strain ratio	Maximum strain	Cycle number	Diameter/mm
24	0.65	0.2	0.0081	10415	5.5
25	0.65	0.2	0.0081	22531	5.5
26	0.65	0.2	0.0081	24563	5.5
27	0.65	0.2	0.0081	59511	5.5
28	0.65	0.2	0.0081	49963	5.5
29	0.65	0.2	0.0081	10790	5.5
30	0.65	0.2	0.0081	61160	5.5
31	0.65	0.2	0.0081	71581	5.5
32	0.752	0.2	0.0094	7231	5.5
33	0.752	0.2	0.0094	9815	5.5
34	0.752	0.2	0.0094	7651	5.5
35	0.752	0.2	0.0094	9986	5.5
36	0.752	0.2	0.0094	5053	5.5
37	0.752	0.2	0.0094	11246	5.5
38	0.752	0.2	0.0094	6865	5.5
39	0.752	0.2	0.0094	90839	5.5
40	0.848	0.2	0.0106	5961	5.5
41	0.848	0.2	0.0106	5462	5.5
42	0.848	0.2	0.0106	9946	5.5
43	0.848	0.2	0.0106	3724	5.5
44	0.848	0.2	0.0106	6999	5.5
45	0.848	0.2	0.0106	6652	5.5
46	0.848	0.2	0.0106	4927	5.5

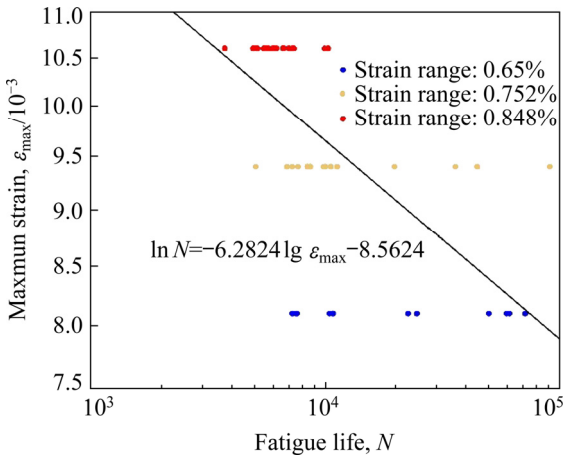

Fig. 3 Fitting curve of FGH96 damage parameters at 600 °C

3 Model verification of crack initiation life of powder superalloy without inclusions

3.1 Derivation of life calculation formula

The fatigue test conditions were constant amplitude-controlled displacement loading, and standard smooth test specimens of powder superalloy FGH96 were used. For the damage evolution Eq. (13), the integral of the life interval (D=0−1) is expressed as

$$\int_0^1 \mathrm{d}D=\int_0^{N_\mathrm{f}} a(Y_\mathrm{max}^{m/2}\mp Y_\mathrm{min}^{m/2})\mathrm{d}N=\int_0^{N_\mathrm{f}} aRY_\mathrm{max}^{m/2}\mathrm{d}N=1 \tag{19}$$

After integration, we can get

$$N_\mathrm{f}=\frac{1}{a(Y_\mathrm{max}^{m/2}\mp Y_\mathrm{min}^{m/2})}=1/\left(\mathrm{a}RY_\mathrm{max}^{m/2}\right) \tag{20}$$

Among them, the cyclic characteristic factor R has been calculated according to the definition in Eq. (12), and when the strain ratio is 0.05, R≈1. The damage parameters m and a of the FGH96 material at 530 and 600 °C have been fitted by the experimental data, as described in Section 2.2. Generally, the characteristic parameters Y_max and Y_min of peak load or valley value can be calculated by finite element method. Therefore, after substituting specific damage parameters into Eq. (20), the life prediction formula of FGH96 material under the pulsating (R≈1) constant amplitude load at 530 and 600 °C can be specifically written as the function of the characterization parameter displacement load peak and valley, respectively:

$$N_{530^\circ\mathrm{C}}=\frac{10^7}{3.8702RY_\mathrm{max}^{2.797}}=\frac{10^7}{3.8702(Y_\mathrm{max}^{2.797}\mp Y_\mathrm{min}^{2.797})} \tag{21a}$$

$$N_{600^\circ\mathrm{C}}=\frac{10^8}{9.1442RY_\mathrm{max}^{3.141}}=\frac{10^8}{9.1442(Y_\mathrm{max}^{3.141}\mp Y_\mathrm{min}^{3.141})} \tag{21b}$$

There are no significant stress−strain concentrations for the case of no meso defects in the material, especially for standard smooth specimens. The nominal stress−strain load can be considered to be uniformly distributed throughout the specimen subjected to uniaxial stress. The maximum characterization parameter Y_max can be degraded to

$$Y_\mathrm{max}=\frac{1}{2}E\varepsilon_\mathrm{max}^2=\frac{E\Delta\varepsilon^2}{2(1-r)^2} \tag{22}$$

where $\Delta\varepsilon$ is the strain range ($\Delta\varepsilon=\varepsilon_\mathrm{max}-\varepsilon_\mathrm{min}$) and r is the cyclic strain ratio ($r=\varepsilon_\mathrm{min}/\varepsilon_\mathrm{max}$).

Substituting Eq. (22) into Eq. (21), we get

$$N_{530^\circ\mathrm{C}}=\frac{(1-r)^{5.594}\times10^7}{3.8702\left(1-r^{5.594}\right)\left(E\Delta\varepsilon^2/2\right)^{2.797}} \tag{23a}$$

$$N_{600^\circ\mathrm{C}}=\frac{(1-r)^{6.282}\times10^8}{9.1442\left(1-r^{6.282}\right)\left(E\Delta\varepsilon^2/2\right)^{3.141}} \tag{23b}$$

This formula is the life calculation formula of the standard smooth test piece of FGH96 material under the constant amplitude loading of controlled strain (displacement) when the cyclic strain ratio is greater than 0 (under tension−tension load).

3.2 Life prediction of specimens without inclusions at 530 and 600 °C

The original fatigue test data of specimens without inclusions at 530 °C are listed in Table 1. Three experimental strain ranges (0.95%, 0.76% and 0.846%), the strain ratio (r=0.05) and the cycle elastic modulus of FGH96 material at this temperature (E=185.3 GPa) were substituted into Eq. (23) to calculate the theoretical prediction life under these three loadings. The predicted results and the average of the experimental life are listed in Table 3 for comparison.

It can be seen from Table 3 that the damage mechanics model proposed in this work has a good effect on predicting the low-cycle fatigue life of FGH96 material with a strain ratio of 0.05 at

Table 3 Prediction results of damage mechanics model of FGH96 without inclusions at 530 °C

Strain ratio, *r*	Strain range/%	Experimental life	Predictive life	Error/ %
0.05	0.95	4807	5105	6
0.05	0.76	19241	17781	−8
0.05	0.846	10544	9765	−7

530 °C, and the deviation between the predicted life and the experimental life is within 10%.

Similarly, the theoretical prediction life of specimens without inclusions at 600 °C was calculated with the original data, as listed in Table 2. The experimental loadings were: strain ranges (0.65%, 0.752% and 0.848%), the strain ratio (r=0.2) and the cycle elastic modulus (E=185.3 GPa). The maximum error of comparison shown in Table 4 is within 20%, which gives an acceptable agreement between the prediction and testing.

Table 4 Prediction results of damage mechanics model of FGH96 without inclusions at 600 °C

Strain ratio, *r*	Strain range/%	Experimental life	Predictive life	Error/ %
0.2	0.65	33671	37025	10
0.2	0.752	18348	14819	−19
0.2	0.848	6206	6967	12

4 Model verification of crack initiation life of powder superalloy with inclusions

The presence of inclusions in powder superalloy FGH96 specimens will cause local stress and strain concentration. The stress and strain at the critical point of crack initiation is different from the nominal stress and strain loaded. Therefore, the nominal stress and strain cannot be used directly to calculate the life. The local stress−strain field has to be obtained through theoretical or numerical computation so that the distribution of the characterization parameter Y can then be calculated.

In the model verification process, the material parameters need to be set according to the specific conditions of the test piece used in the experiment. A soft inclusion was considered if the inclusion was a mixed component of a plurality of objects, and its elastic modulus was lower than that of the powder superalloy matrix according to the measurement results by the nanoindentation method. The elastic modulus in this case was taken as 150 GPa in the calculation and the Poisson's ratio was 0.3. If the inclusion component was pure metallic alumina, its elastic modulus was higher than that of the powder superalloy matrix, and it was considered as a hard inclusion. The elastic modulus was taken as 400 GPa in the calculation and the Poisson's ratio was 0.3. The matrix material was FGH96 material, which adopted the classical elastoplastic constitutive equation, and its average tensile stress−strain equation was

$$\frac{\Delta\varepsilon}{2}=\frac{\Delta\sigma}{2E}+\left(\frac{\Delta\sigma}{2K}\right)^{1/n} \tag{24}$$

where the elastic modulus E=185.3 GPa, the hardening coefficient K=2702.7 MPa, the hardening index n=0.144, and Poisson's ratio v=0.35.

PLANE82 element in ANSYS finite element software was used in finite element modeling. Structured grids were used as much as possible in mesh generation, while less random grids could improve the accuracy and efficiency of computation. The mesh should be densified in the part containing inclusions. When the load is applied, the equivalent displacement should be calculated according to the actual loading situation. The geometric parameters of the finite element calculation model need to be simplified and selected according to the actual pre-test piece and geometric characteristics of their inclusions. Most inclusions had approximately ellipsoidal shapes and could be simplified to elliptical inclusion model. However, some inclusions were exposed to the surface of the test specimens as surface inclusions; while others were at a certain distance from the surface and could be considered as subsurface inclusions. For inclusions with relatively sharp-angled contours on the surface, it could be simplified to a strip-shaped inclusion model.

4.1 Life prediction of specimen with elliptical subsurface inclusions

Figure 4 shows the scanning electron micrograph of the tested Specimen A1, which indicates that the crack initiation site contained a mixed inclusion mainly composed of Al_2O_3. It was measured as an elliptical inclusion with a major axis of 63 μm and a minor axis of 61 μm. The

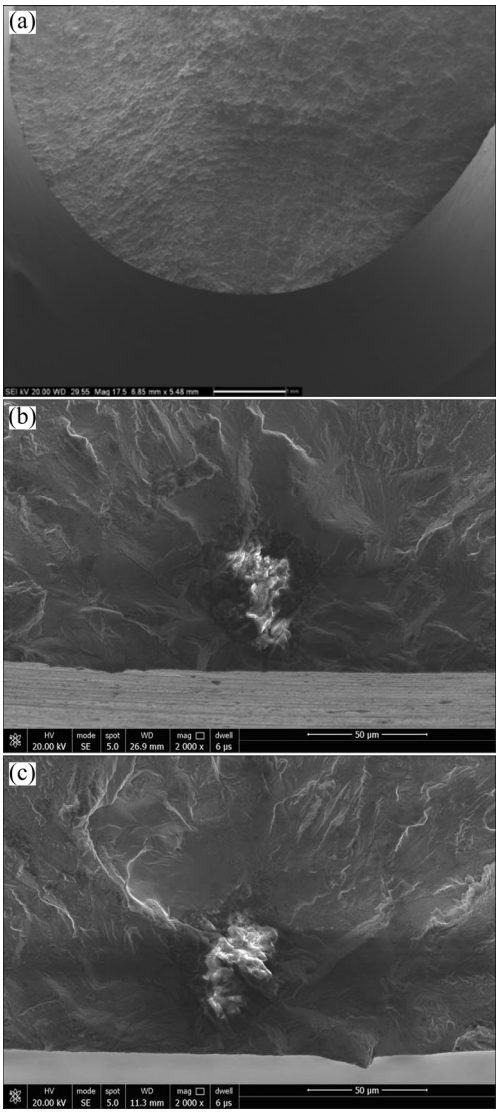

Fig. 4 Microscopic morphologies of Specimen A1: (a) Macro fracture morphology; (b, c) Crack source area

inclusions were subsurface inclusions 0.04 mm away from the surface of the tested piece.

In the finite element modeling, it was simplified to a circle with a radius of 30 μm and a distance of 0.04 mm from the surface of the specimen. The specimen was simulated as a 1/2 symmetrical model with a width of 6 mm and a height of 3 mm.

The local mesh of the finite element model is shown in Fig. 5.

Since the load was a constant strain load, the calculation showed that when the strain range was 0.846% and the strain ratio was 0.05, the maximum displacement of the upper and lower ends of the specimen was 0.0267 mm. In the finite element model, the upper surface was stretched by 0.0267 mm along the *y*-axis by applying displacement boundary conditions. A symmetric boundary condition was applied to the symmetric surface to solve the problem.

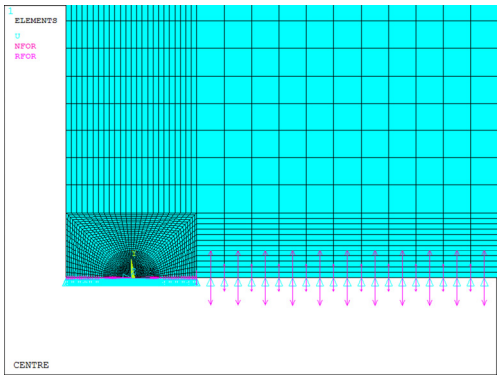

Fig. 5 Mesh generation of inclusion in Specimen A1

After strain components of each element were extracted, the distribution of damage characterization parameter Y could be calculated according to the Eq. (10), as shown in Fig. 6, where the crack initiation position was located on both sides of the inclusion, and the maximum characterization parameter was 8.3898. According to Eq. (21a), the life expectancy was calculated to be 6738 cycles, while the experimental results showed that the life of the specimen was 8125 cycles. The prediction error is about 17%.

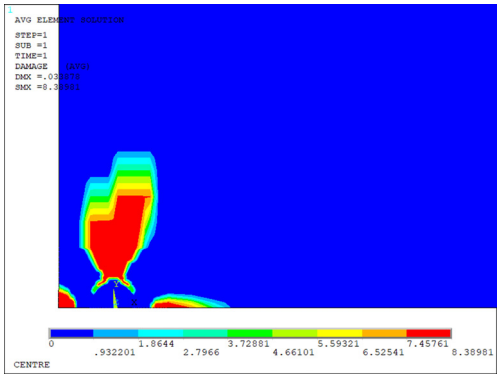

Fig. 6 Distribution of damage characterization parameter in Specimen A1

4.2 Life prediction of specimens with elliptical surface inclusions

Take Specimen A3 as an example to illustrate the life calculation process of specimen with elliptical surface inclusions. The crack initiation site contained a mixed inclusion mainly composed of Al_2O_3 and SiO_2. The elliptical surface inclusion size was measured, as shown in Fig. 7, which had a

major axis of 102 μm and a minor axis of 54 μm. The local mesh of the finite element model is shown in Fig. 8. The calculated distribution of damage characterization parameter is shown in Fig. 9. The predicted life was around 6115 cycles, which is comparable with the experimental life of 6276 cycles.

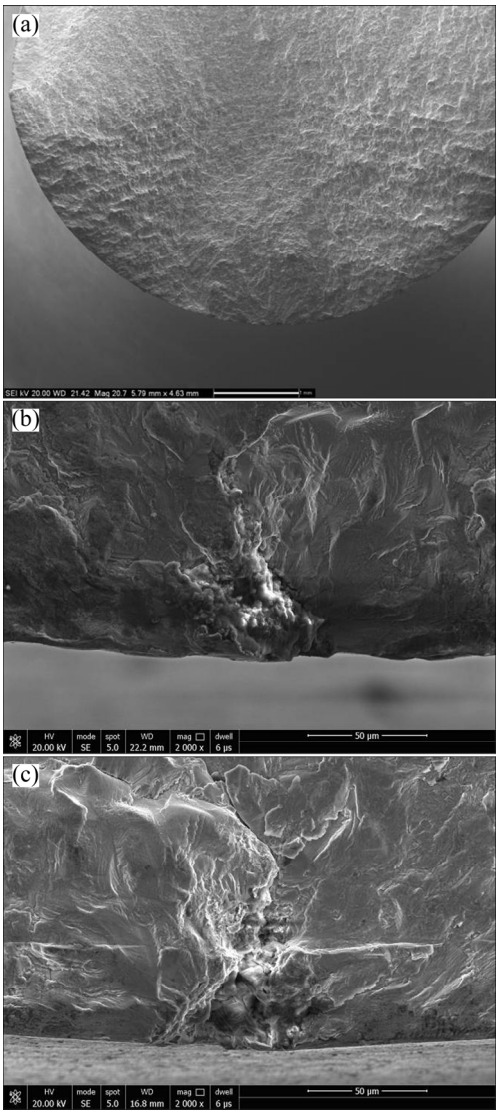

Fig. 7 Microscopic morphologies of Specimen A3: (a) Macro fracture morphology; (b, c) Crack source area

4.3 Life prediction of specimens with strip-shaped subsurface inclusions

The strip-shaped subsurface inclusions of Specimen A4 were also considered. Firstly, the modeling of the shape and characteristics of the inclusions in the specimen was simplified. The scanning electron micrograph in Fig. 10 shows a mixed inclusion mainly composed of Al_2O_3 and SiO_2. Such a strip-shaped subsurface inclusion was

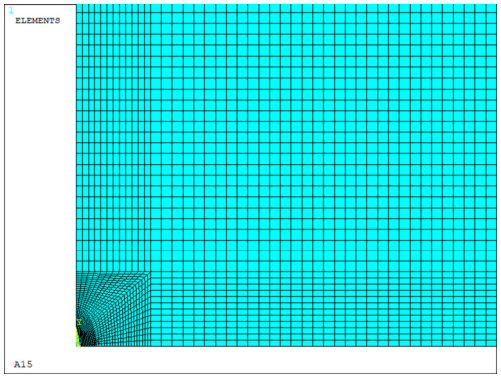

Fig. 8 Mesh generation of inclusions in Specimen A3

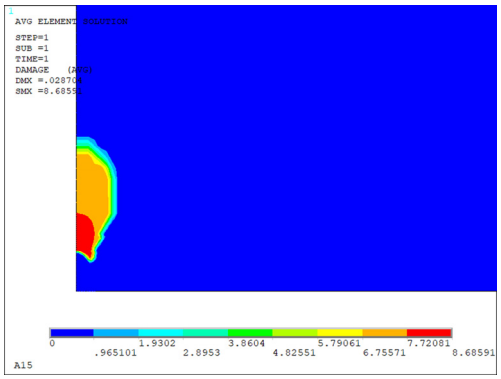

Fig. 9 Distribution of damage characterization parameter in Specimen A3

measured to have a major axis of 87 μm and a minor axis of 13 μm, with a depth of 0.047 mm from the surface. The local mesh of the finite element model is shown in Fig. 11.

According to Eq. (21a) and Fig. 12, the calculated life expectancy is 8231 cycles, which has an error of 26% compared with the experimental average life of 11116 cycles for the specimen.

5 Group testing and effects of life prediction

According to the method above, three sets of specimens containing different sizes, positions and shapes of inclusions with different temperatures, different strain ranges (loads) and different strain ratios were selected to verify the life prediction model.

(1) First group

In the first group, five specimens containing inclusions were selected for life prediction. The experimental conditions were T=530 °C, strain range 0.846%, and strain ratio r=0.05. The specific information is listed in Table 5. The theoretical life

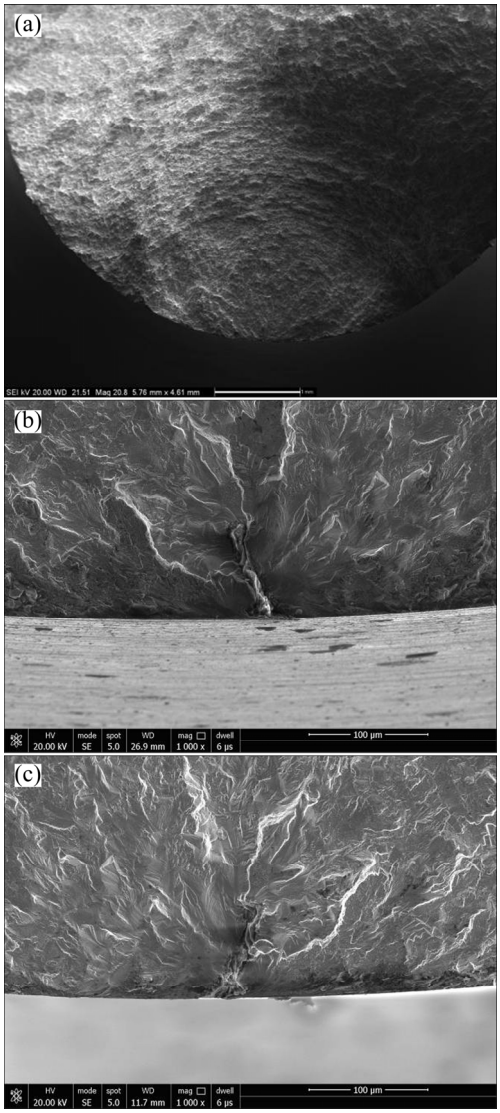

Fig. 10 Microscopic morphologies of Specimen A4: (a) Macro fracture morphology; (b, c) Crack source area

of these specimens was calculated using the aforementioned life prediction model. The comparison between the predicted results and the experimental results is shown in Table 6. It is noted that large errors occur in the shape modelling of inclusions, with strip and polygon types illustrating

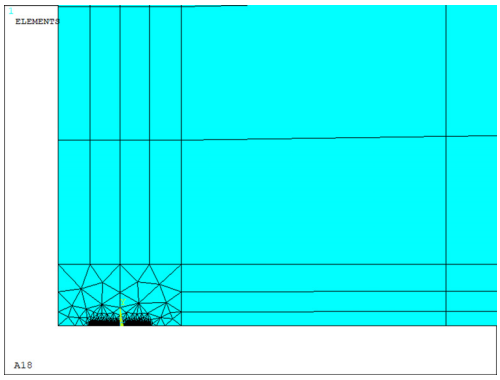

Fig. 11 Mesh generation of inclusions in Specimen A4

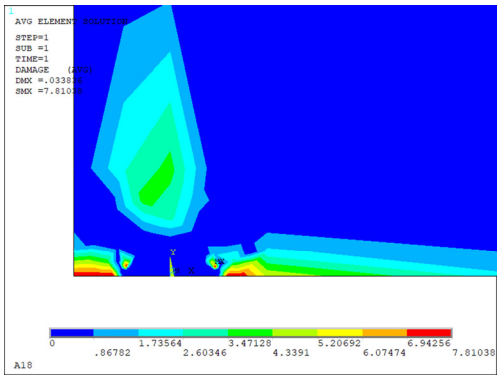

Fig. 12 Distribution of damage characterization parameter in Specimen A4

them to be sensitive to the predication of fatigue life.

(2) Second group

The testing conditions in the second group were T=600 °C, strain range 0.752%, and strain ratio r=0.2. From Table 7 and Table 8, it can be observed that the inclusion shapes affect the prediction accuracies, particularly with strip and semi-elliptic shapes. The 48% prediction error suspects the aforementioned life prediction model.

(3) Third group

Experimental conditions of the third set were T=530 °C. Since the load was a constant strain load, the calculation showed that when the strain range

Table 5 Experimental data of first group

Specimen	Cycle No.	Diameter/mm	Main component of defect	Source area	2a/μm	2c/μm	Distance between defect and surface/mm
A1	8125	6	Al_2O_3, Co	Elliptic	61	63	0.04
A2	13550	6	Al_2O_3, SiO_2	Elliptic	41	57	0
A3	6276	6	Al_2O_3, SiO_2	Elliptic	102	54	0
A4	11116	6	Al_2O_3, SiO_2	Strip	13	87	0.047
A5	9246	6	Al_2O_3	Polygon	48	66	0

Table 6 Life prediction results of first set

Specimen	Y_{max}	Experimental life	Predicted life	Error/%
A1	8.3818	8125	6738	−17
A2	8.1965	13550	11744	−13
A3	8.6859	6276	6115	−3
A4	7.8104	11116	8231	−26
A5	8.209	9246	7161	−23

was 0.76% and the strain ratio was 0.05, the maximum displacement of the upper and lower ends of the specimen was 0.024 mm. Table 9 lists the specimen information, and the experimental results are given in Table 10. The prediction of semi-elliptic inclusion specimen gives the largest error of 22%.

In summary, by comparison with the experimental life, it is found that the fatigue life model based on damage mechanics has good applicability in the prediction of low-cycle crack initiation life of powder superalloy FGH96. Among the experimental specimens participating in the life prediction calculation, the exceptional highest error is 48%, but the prediction errors for most of the specimens are within 25%.

It is argued that the predicted life errors calculated by finite element simulation may mainly come from two aspects. One is that when non-destructive smooth specimens were used for data fitting, the damage parameters obtained had certain errors, which introduced errors into the life prediction model. The second is that the matrix material and inclusions were simplified into a 2D plane model. This model reduced the number of degrees of freedom of the nodes in finite element meshing, and could not simulate the material interaction of the specimen under loadings in the actual situation. Additionally, when building the model of inclusions, only two sizes of inclusions were used, which did not reflect the actual shapes of the inclusions. Inclusions in other dimensions

Table 7 Experimental data of second group

Specimen	Cycle No.	Diameter/mm	Main component of defect	Source area	$2a$/μm	$2c$/μm	Distance between defect and surface/mm
B1	6293	5.5	Al_2O_3, Zr	Semi-elliptic	94	75	0
B2	7643	5.5	Al_2O_3, SiO_2, TiO	Elliptic	49	41	0
B3	6365	5.5	Al_2O_3, SiO_2, Fe	Elliptic	58	42	0
B4	7546	5.5	Al_2O_3, SiO_2, Mg, Fe	Strip	26	34	0.038
B5	6205	5.5	Al_2O_3, SiO_2, MgO	Elliptic	56	67	0

Table 8 Life prediction results of second group

Specimen	Characterization parameter, Y_{max}	Experimental life	Predicted life	Error/%
B1	10.1662	6293	7505	−19
B2	10.4044	7643	6979	9
B3	10.1714	6365	7493	18
B4	8.9639	7546	11144	48
B5	10.9462	6205	5950	−4

Table 9 Experimental data of third group

Specimen	Cycle No.	Diameter/mm	Main component of defect	Source area	$2a$/μm	$2c$/μm	Distance between defect and surface/mm
C1	14817	6	Al_2O_3, SiO_2	Triangle	68	56	0
C2	11387	6	Al_2O_3, SiO_2, TiO	Semi-elliptic	91	59	0
C3	15368	6	Al_2O_3, SiO_2	Elliptic	44	52	0.036
C4	14666	6	Al_2O_3, SiO_2	Polygon	48	30	0
C5	9584	5.5	Al_2O_3	Elliptic	72	23	0

Table 10 Life prediction results of third group

Specimen	Y_{max}	Experimental life	Predicted life	Error/ %
C1	6.3462	14817	14711	−1
C2	6.4742	11387	13912	22
C3	6.5132	15368	13680	−11
C4	6.2852	14666	14666	0
C5	7.5888	9584	8921	−7

may have accountable effects on errors between the experimental life and the predicted life.

6 Conclusions

(1) The testing results show that the proposed damage characterization parameters can meet the need of characterizing the low-cycle fatigue damage of the material, and is suitable for specimens with and without inclusions.

(2) The fatigue life prediction model of powder superalloy FGH96 established is suitable for experimental conditions of different temperatures, different strain ranges and different strain ratios. For specimens without inclusions, the fatigue life error is within 20%. This shows that temperature, strain range and strain ratio have little effect on the fatigue life prediction of powder superalloy FGH96.

(3) Through finite element calculations, it can be found that the shape, location and size of inclusions all have influence on the fatigue life of the powder superalloy, and the shape of the inclusions is the most critical factor.

Acknowledgments

This work was sponsored by AECC Beijing Institute of Aeronautical Materials, and was funded by National High-tech R&D Program of China (863 Program) (No. 2015AA034401).

References

[1] TIAN Qing-hua, GAN Xiang-dong, YU Da-wei, CUI Fu-hui, GUO Xue-yi. One-step and selective extraction of nickel from nickel-based superalloy by molten zinc [J]. Transactions of Nonferrous Metals Society of China, 2021, 31(6): 1828−1841.

[2] JIANG R, SONG Y D, REED P A. Fatigue crack growth mechanisms in powder metallurgy Ni-based superalloys—A review [J]. International Journal of Fatigue, 2020, 141: 105887.

[3] CHEN S Y, WEI D S, WANG J L, WANG Y R, JIANG X H. Experimental and modeling investigation of the creep−fatigue interactive deformation behavior of PM superalloy FGH96 at evaluated temperature [J]. Materials Science and Engineering A, 2019, 749: 106−117.

[4] JIANG J, YANG J, ZHANG T, ZOU J, WANG Y, DUNNE F P E, BRITTON T B, Microstructurally sensitive crack nucleation around inclusions in powder metallurgy nickel-based superalloys [J]. Acta Materialia, 2016, 117: 333−344.

[5] DOWLING N E. Mechanical behavior of materials: Engineering methods for deformation, fracture, and fatigue [M]. Pearson, 2012.

[6] LIU Xin-ling, TAO Chun-hu. Research progress and analysis on defect characteristic and life estimation of powder metallurgy superalloy [J]. Materials Review, 2013, 27: 92−96.

[7] MANSON S S. Behaviour of materials under condition of the thermal stress [S]. NACA TN-2933, 1954.

[8] COFFIN L F. A Study of the effects of cyclic thermal stresses on a ductile metal [J]. Transactions of the American Society of Mechanical Engineers, 1954, 76: 931−950.

[9] HU Dian-yin, WANG Tao, MA Qi-hang, LIU Xi, SHANG Li-hong, LI Da, PAN Jin-chao, WANG Rong-qiao. Effect of inclusions on low cycle fatigue lifetime in a powder metallurgy nickel-based superalloy FGH96 [J]. International Journal of Fatigue, 2019, 118: 237−248.

[10] CHEN Yong. Research on crack propagation life of turbine disk containing inclusion powder superalloy [D]. Nanjing University of Aeronautics and Astronautics, 2003. (in Chinese)

[11] MIAO Guo-lei, YANG Xiao-guang, SHI Duo-qi. Competing fatigue failure behaviors of Ni-based superalloy FGH96 at elevated temperature [J]. Materials Science and Engineering, A, 2016, 668: 66−72.

[12] CASHMAN G T. A statistical methodology for the preparation of a competing modes fatigue design curve [J]. Journal of Engineering Materials and Technology, 2007, 129(1): 159−168.

[13] BARRIE R L, GABB T P, TELESMAN J, KANTZOS P T, PRESCENZI A, BILES T, BONACUSE P J. Effectiveness of shot peening in suppressing fatigue cracking at non-metallic inclusions in Udimet 720 [J]. Materials Science and Engineering, A, 2008, 474: 71−81.

[14] JHA S. Collaborative research and development (CR&D) delivery order 0037: Mechanisms causing fatigue variability in turbine engine materials [M]. Dayton (OH): Universal Technology Corp, 2008.

[15] ZHU Shun-peng, HUANG Hong-zhong, PENG Wei-wen, WANG Hai-kun, MAHADEVAN S. Probabilistic physics of failure-based framework for fatigue life prediction of aircraft gas turbine discs under uncertainty [J]. Reliability of Engineering and System Safety, 2016, 146: 1−12.

[16] ZHU Shun-peng, HUANG Hong-zhong, SMITH R, ONTIVEROS V, HE Li-ping, MODARRES M. Bayesian framework for probabilistic low cycle fatigue life prediction and uncertainty modeling of aircraft turbine disk alloys [J]. Probabilistic Engineering Mechanics, 2013, 34: 114−122.

[17] ZHU Shun-peng, HUANG Hong-zhong, ONTIVEROS V,

HE Li-ping, MODARRES M. Probabilistic low cycle fatigue life prediction using an energy-based damage parameter and accounting for model uncertainty [J]. International Journal of Damage Mechanics, 2012, 21(8): 1128−1153.

[18] JIANG R, EVERITT S, GAO N, SOADY K, BROOKS J W, REED P A S. Influence of oxidation on fatigue crack initiation and propagation in turbine disc alloy N18 [J]. International Journal of Fatigue, 2015, 75: 89−99.

[19] JIANG R, EVERITT S, LEWANDOWSKI M, GAO N, REED P A S. Grain size effects in a Ni-based turbine disc alloy in the time and cycle dependent crack growth regimes [J]. International Journal of Fatigue, 2014, 62: 217−227.

[20] SONG Yin-dong, GAO De-ping. Probability method for fatigue life of powder metallurgy disk based on inclusion distribution [J]. Aero Engine, 1998(2): 49−52. (in Chinese)

[21] ZHANG Peng, ZHU Qiang, CHEN Gang, QIN He-yong, WANG, Chuan-jie. Grain size based low cycle fatigue life prediction model for nickel-based superalloy [J]. Transactions of Nonferrous Metals Society of China, 2018, 28(10): 2102−2106.

[22] ROSENBERGER A H, GHONEM H. High temperature elastic−plastic small crack growth behavior in nickel-base superalloy [J]. Fatigue & Fracture of Engineering Materials & Structures 1994, 17(5): 509−521.

[23] PELLOUX R, FENG J, ROMANOSKI G. A study of the fatigue behavior of small cracks in nickel-base superalloys [R]. Cambridge MA: AFOSR-TR, 1988, 0457.

[24] CHAN K S. A fatigue life model for predicting crack nucleation at inclusions in Ni-based superalloys [J]. Metallurgical and Materials Transactions A − Physical Metallurgy and Materials Science, 2020, 51: 1148−1162.

[25] SHI Yi, YANG Xiao-guang, YANG Di-di, SHI Duo-qi, MIAO Guo-lei, WANG Zhi-fang. Evaluation of the influence of surface crack-like defects on fatigue life for a P/M nickel-based superalloy FGH96 [J]. International Journal of Fatigue, 2020, 137: 105639.

[26] ZHANG Xing. Fracture and damage mechanics [M]. Beihang University Press, 2009. (in Chinese)

基于损伤力学的含夹杂粉末高温合金 FGH96 低周裂纹萌生寿命预测

徐元铭[1]，张书明[1]，贺天鹏[1]，刘新灵[2]，常夏源[1]

1. 北京航空航天大学 航空科学与工程学院，北京 100191；
2. 中国航发北京航空材料研究所，北京 100095

摘　要：研究 FGH96 粉末高温合金中夹杂物对低周疲劳寿命的影响，提出基于损伤力学理论的低周裂纹萌生寿命预测模型，在建立损伤演化方程后提出损伤表征参数。对含夹杂物和不含夹杂物的粉末高温合金试样在 530 ℃和 600 ℃下进行疲劳试验，并对具有椭圆形、半椭圆形、多边形和条形表面/亚表面夹杂物的试样进行模型验证，然后通过有限元模拟进行应力分析，并计算预测寿命。结果表明，预测寿命和实验寿命之间具有令人满意的一致性。

关键词：粉末高温合金 FGH96；低周疲劳；夹杂；裂纹萌生寿命预测；损伤力学

(Edited by Bing YANG)